Supplementary Information (SI) for RSC Applied Interfaces.

Electronic Supporting Information

for

A soft approach towards composite porous carbon/conducting polymer supercapacitors: layer-by-layer integration of pyrolyzed ZIF-8 MOF and PANI-PSS supramolecular complexes

Ana Paula Mártire,[a] Omar Azzaroni,[a] Waldemar Marmisolle,[a]* and Matias Rafti[a]*

a. Instituto de Investigaciones Fisicoquímicas Teóricas y Aplicadas (INIFTA Departamento de Química, Facultad de Ciencias Exactas, Universidad Nacional de La Plata-CONICET, La Plata B1904DPI, Argentina. E-mail: wmarmi@infita.unlp.edu.ar; mrafti@quimica.unlp.edu.ar.

S1. Characterization of ZIF-8 colloids

Crystalline structure was determined using wide-angle X-ray scattering (WAXS) on powdered samples. The SAXS/WAXS system (INIFTA, "Nanopymes"-EuropeAid/132184 D/SUP/AR Contract 331-896) is a XEUSS 1.0 HR (XENOCS, Grenoble) equipped with a microfocus X-ray source and a Pilatus 100 K detector (DECTRIS AG, Switzerland). Fig. S1 shows the measured WAXS for the ZIF-8 dry sample and the comparison with the calculated peaks. The coincidence between the graphs indicates the presence of the ZIF-8 phase.

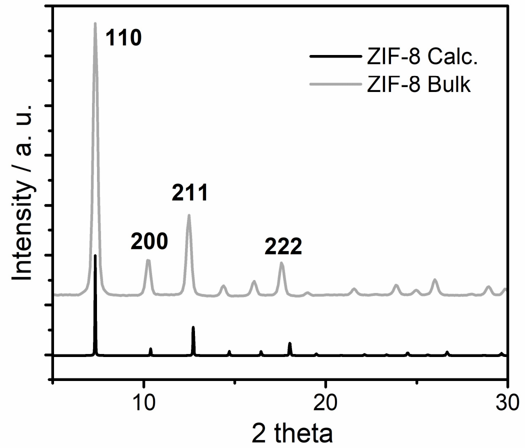

Figure S1- WAXS pattern of ZIF-8: in grey for the colloids obtained in the lab and, in black the theoretical diffraction pattern calculated with data from Cambridge Crystallographic Data Centre (CCDC).

Thermal degradation of ZIF-8 was assessed using a TA Instruments equipment (TGA Q500) (Fig. S2). The sample was heated applying a 10 °C min^{-1} rate under a 40 mL min^{-1} N_2 flux. It is observed that the thermal stability of the ZIF-8 remains until 450 °C when the degradation begins.

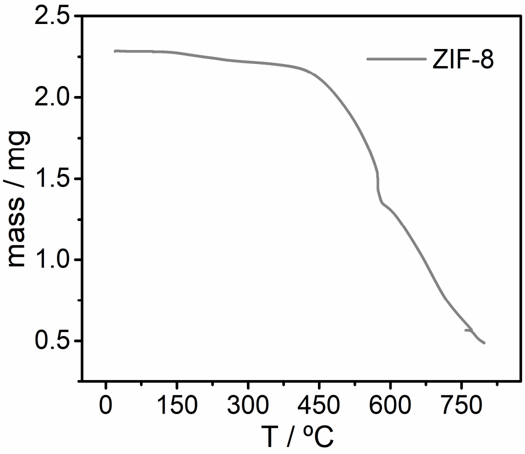

Figure S2- Thermogram of ZIF-8 in N_2 atmosphere.

S2. Adsorption analysis of ZIF-8 and PCZIF-8

Adsorption of N_2 at 77K was performed in previously activated samples. The isotherms are shown in Fig. 1B. To obtain the surficial area, first, the data was analysed by Rouquerol's plot (Fig S3 A and, B).[1,2] The appropriate range of pressures was selected in these plots, considering that $W(1-P/P_0)$ increases monotonically with P/P_0. Next, the linearized BET plot was done (Fig. S3 C and, D).[3] The parameter Wm was obtained, which is the weight of the adsorbed monolayer by applying Eq. S1

$$\frac{1}{W\,(\frac{P_0}{P}-1)} = \frac{1}{C\,W_m} + \frac{C-1}{CW_m}\,(\frac{P}{P_0}) \qquad \text{(S1)}$$

In this equation, C is the BET constant. Then, the specific surface area was calculated by applying Eq. S2:

$$S\,(m^2g^{-1}) = \frac{W_m N_a A_{N2} 10^{-20}}{M_{N2}} \qquad \text{(S2)}$$

Where N*a* is Avogadro's number, A_{N2} is the cross-section of the molecule (16.2 A^2) and M_{N2} is the molar mass of N_2 (28.013 g mol^{-1}). The BET surface area is 1473 m^2 g^{-1} for ZIF-8 agreeing with previous reports.[4] For PCZIF-8 a BET surface area of 875 m^2 g^{-1} determined calculated.

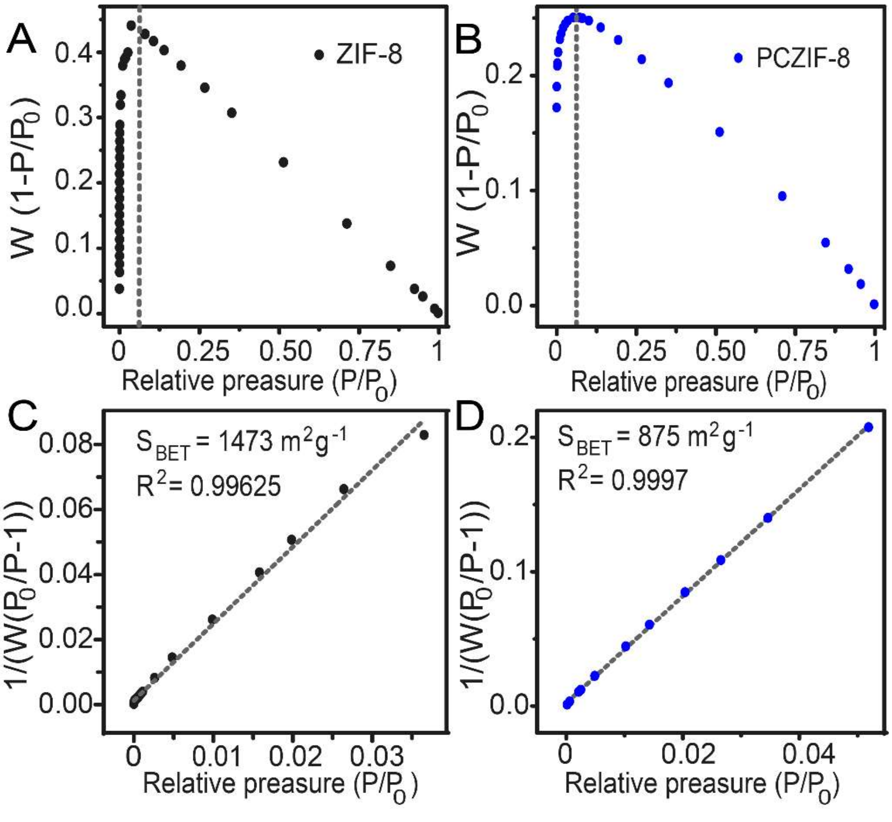

Figure S3 - Rouquerol's plot for **(A)** ZIF-8 and **(B)** PCZIF-8. The dotted line delimits the chosen region. Linearized BET plot for **(C)** ZIF-8 and **(D)** PCZIF-8.

S3. Electrochemical growth of the films

The PANI-PSS/PCZIF-8 assembly was conducted in the Teflon electrochemical cell to test the electroactivity and electrochemical connectivity of the film. Cyclic voltammograms were recorded after each PANI-PSS step deposition. Fig. S4 shows the response for this LbL assembly in 0.1M KCl. As observed in HCl, the current increased after each deposition step.

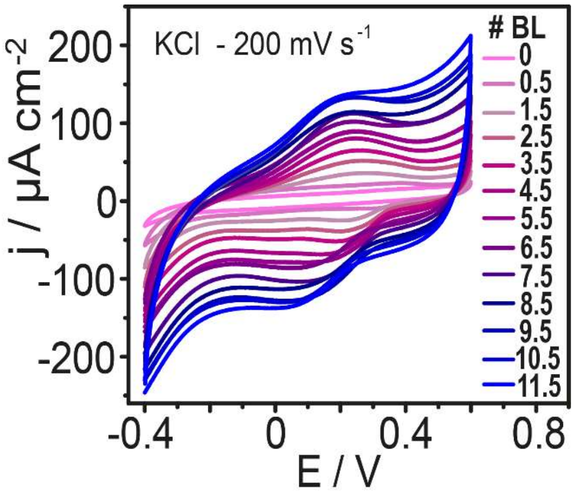

Figure S4 – Cyclic voltammetry response for the growing film for the PANI-PSS/PCZIF-8 assembly in 0.1M KCl

The same procedure was performed constructing an LbL film with graphitic carbon (GC). Fig. S5 A and B exhibit the voltammograms obtained after each PANI-PSS step deposition in HCl, and KCl. After each deposition step, the current grows, but the achieved current value is lower for the assembly with no carbon porosity.

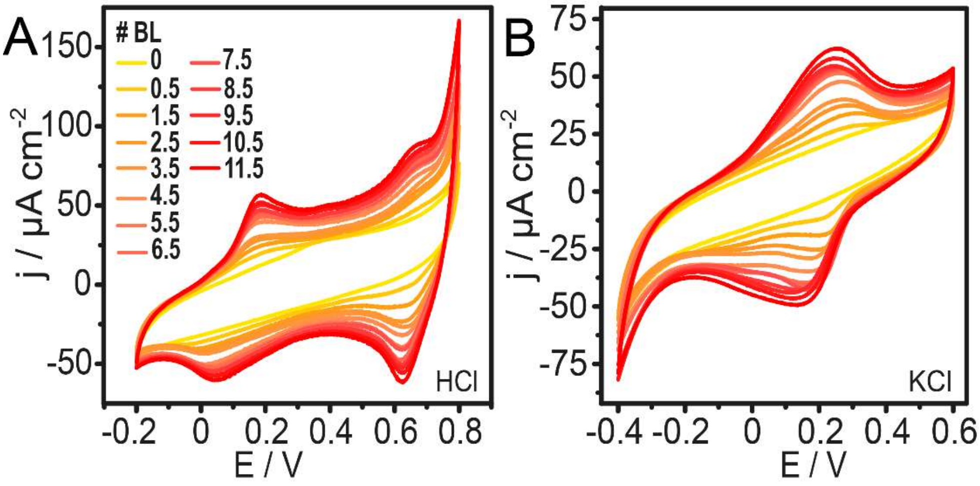

Figure S5 - Cyclic voltammetry measurements for the PANI-PSS/GC growing assembly at 200 mV s^{-1} in 0.1M HCl **(A)** and 0.1M KCl **(B)**.

S4. Comparison of the GC and PCZIF-8 films

To evaluate the carbon porosity contribution to the capacity of the assembly, PANI-PSS/PCZIF-8 was compared with an assembly prepared with commercial graphitic carbon, PANI-PSS/GC. The response for 11.5 bilayers of both assemblies in 0.1M KCl is shown in Fig.S6. Notably, the carbon porosity enhances the electrochemical response of the film.

To further analyse their electrochemical response, the specific voltammetric capacitance was calculated from both assemblies. The contrast in the electrochemical performance of the two systems is more pronounced when specific capacitance is compared. Table S1 displays specific voltammetric capacitance for 11.5 bilayer films at different scan rates. Next, Fig. S7 shows $C_{CV,SP}$ values for increasing bilayers of the two assemblies at 200 mV s^{-1}. The difference in these two cases, in $C_{CV,SP}$ values, is substantial, since the PCZIF-8 assembly has a lower mass and outperforms the GC assembly electrochemically

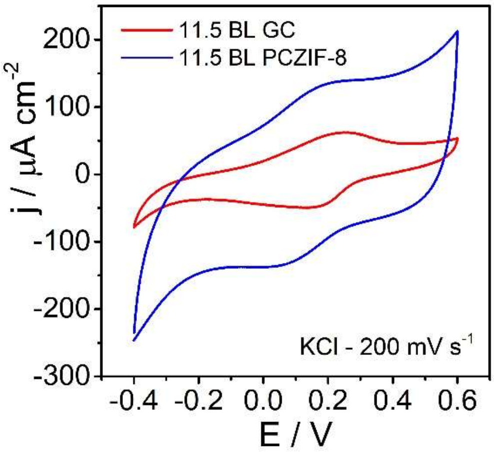

Figure S6 - Voltammograms for 11.5 BL for the assembly PANI-PSS/PCZIF-8 and PANI-PSS/GC in 0.1 M KCl.

Table S1 – Comparison of specific capacitance values for PANI-PSS/PCZIF-8 and PANI-PSS/GC for 11.5BL assemblies.

Scan rate (mV s-1)	Csp (F g-1) - PANI-PSS/PCZIF-8		Csp (F g-1) - PANI-PSS/GC	
	0.1 M HCl	0.1 M KCl	0.1 M HCl	0.1 M KCl
10	163.3	110.7	12.8	13.8
50	127.6	71.5	9.9	4.9
100	114.6	59.5	8.8	4.3
200	102.4	49.5	8.3	4.0
500	86.9	38.8	8.1	4.0
1000	74.6	30.1	8.0	4.0

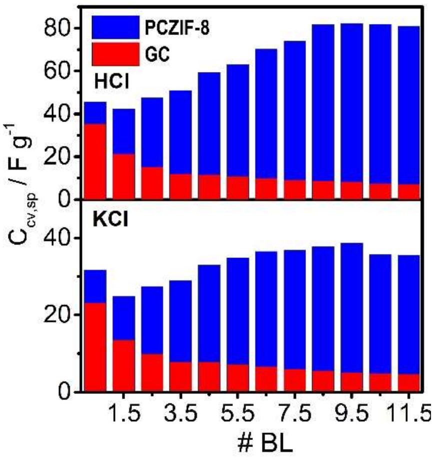

Figure S7 -. Specific voltammetric capacitance values with increasing bilayers in the assembly process for PCZIF-8 and GC at 200mV s^{-1}

S5. Analysis of the capacitance components

To evaluate the *b* values using Dunn's method, plots of log(*j*) versus log(*v*) were constructed, as shown in Figure S8. For these plots, the oxidative branch of the cyclic voltammetry curves was considered, and the current density (*j*) was taken at fixed potentials. The selected potentials are indicated in the figure and correspond to the data used for the calculation of *b*. In this analysis, scan rates of 10, 50, 100, 200, 500, and 1000 mV s^{-1} were considered.

Next, $j/v^{1/2}$ was plotted to obtain the k'_1 and k'_2 values. Figure S9 shows some examples of linear fittings performed for KCl. In this case, scan rates of 10, 50, 100, 200, and 500 mV s^{-1} were considered. Using the obtained k'_1 and k'_2 values, graphical reconstructions of j_c and j_d were carried out for each scan rate and for both electrolytes, as shown in Figure S10.

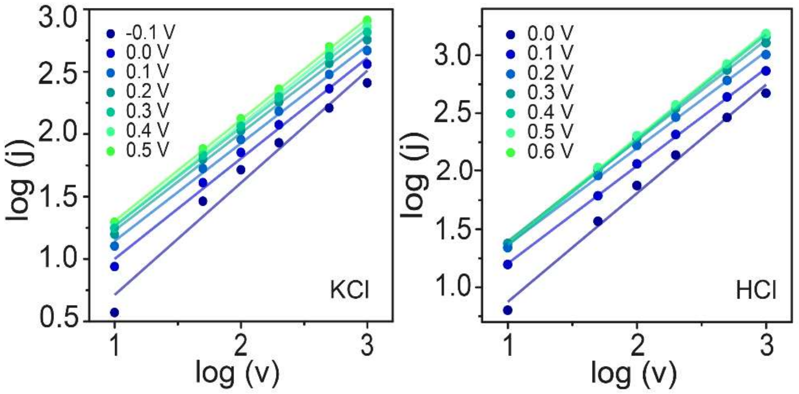

Figure S8 – Linear fittings applied to obtain b value in KCl and HCl.

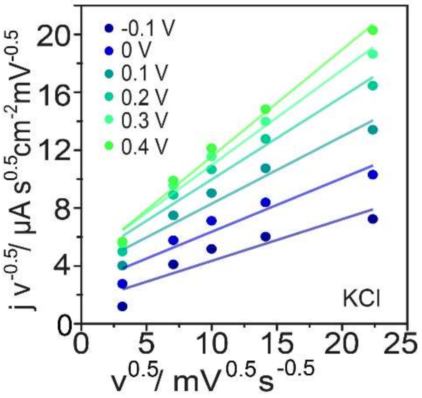

Figure S9 - j $v^{-0.5}$ with $v^{0.5}$ with their linear regression fitting used to obtain k'_1 and k'_2 in 0.1M KCl

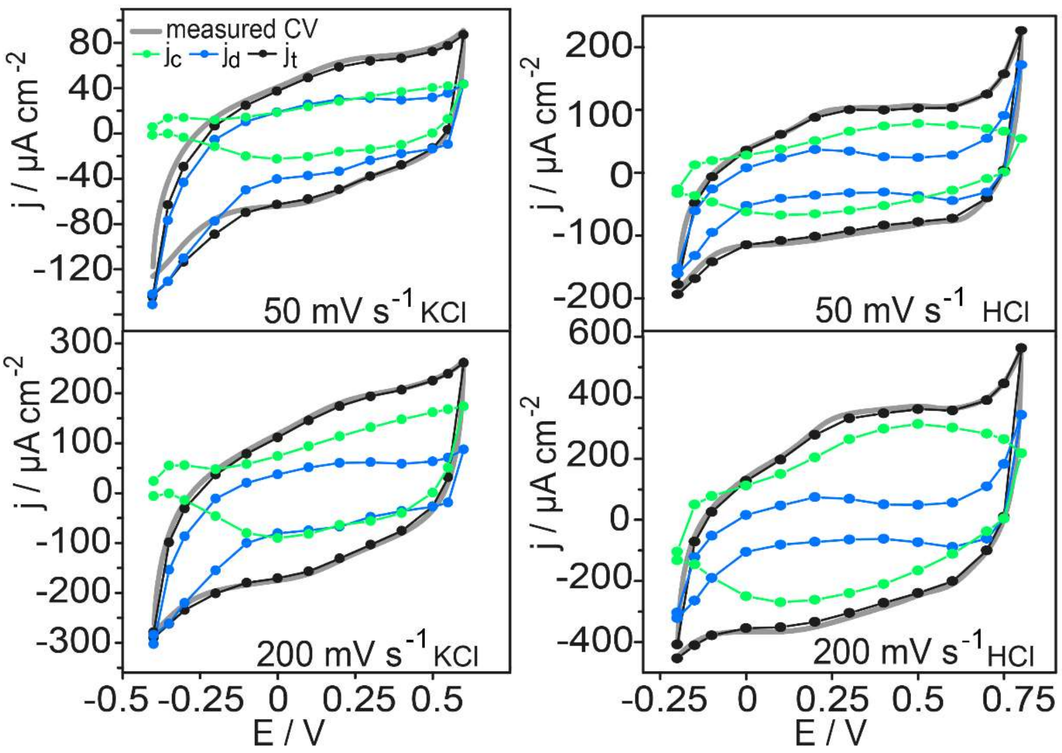

Figure S10 - Cyclic voltammograms for 50 and 200 mV s^{-1} with j_d and j_c contributions

S6. Ionic exchange during cyclic voltammetry

QCM Au sensors were modified using the same procedure as in Fig. 2A. To study the ions and solvent exchange eQCM 10M™ Impedance Scanning Electrochemical Quartz Crystal Microbalance from Gamry Instruments, complementing the Gamry Reference 600 potentiostat, was employed. Fig. S11 shows the result obtained in 0.1M HCl at 200 mV s^{-1}. The mass exchange was calculated by applying the Sauerbray model. Fig. S12 shows the mass exchange measured during the increasing bilayers of the assembly procedure at 200 mV s^{-1} in 0.1M HCl.

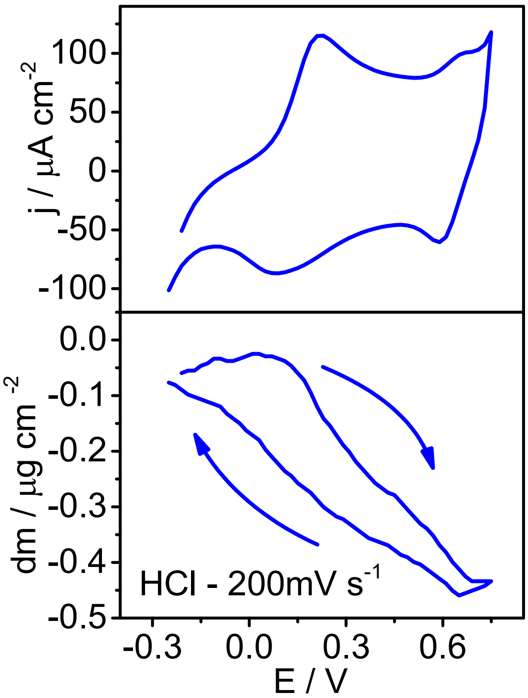

Figure S11 - Cyclic voltammetry and QCM mass change curves for the PANI-PSS/PCZIF-8 assembly in 0.1M HCl at 200 mV s^{-1}.

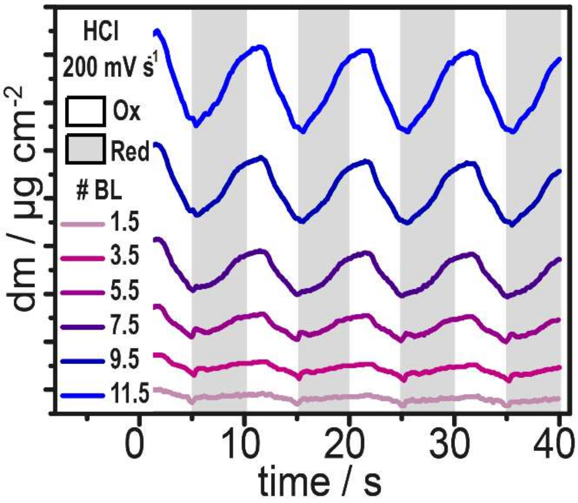

Figure S12 - Mass changes as a function of time during cyclic voltammetry as the number of bilayers increases. Grey regions indicate cathodic scans, whereas white regions correspond to anodic scans.

S7. Bibliographic comparison

To enable further comparison with studies employing similar materials, Table S2 summarizes the results reported for electrodes that include PANI among their components. Reported data correspond to both neutral and acidic electrolytes, where the distinct capacitance values obtained in each medium can be clearly observed.

Table S2- Supercapacitor performance comparison considering electrodes including PANI.

Electrodes using PANI	Electrolyte	Csp (F g-1)	Cycling Stability (GCD o CV)	Reference
PANI-PHQ/RGO	1 M H_2SO_4	356 – 0.5 A g^{-1}	94% - 1000 cycles - 10 A g^{-1}	[5]
RGO-PANI HS	1 M H_2SO_4	456 – 0.5 A g^{-1}	83% - 1000 cycles - 0.5 A g^{-1}	[6]
PANI on rGO paper	1 M H_2SO_4	233 -2 mV s^{-1}	100% -1500 cycles- 2 mV s^{-1}	[7]
PANI nanosphere/rGO film	0.5 M H_2SO_4	448 - 1 A g^{-1}	81% -5000 cycles- 2 A g^{-1}	[8]
PANI/CNTs nanofibers	1 M H_2SO_4	385 - 0.5 A g^{-1}	81.4 %-1000 cycles	[9]
Crystalline PANI by self-stabilised dispersion polymerisation	1 M H_2SO_4 + 0.4 M HQ	438 - 0.5 A g^{-1}	98.3% -8500 cycles- 5 A g^{-1}	[10]
Polyaniline-carbon nanofibers (PANI-PCNFs)	1M Li_2SO_4	65 -2 A g^{-1}	74% - 4500 cycles- 2 A g^{-1}	[11]
Sulfonated-PANI-Carbon cloth	0.5 M Na_2SO_4	65 -1 A g^{-1}	50% - 1000 cycles -2 A g^{-1}	[12]
PANI-Carbon cloth	0.5 M Na_2SO_4	58 - 1 A g^{-1}	30% -1000 cycles- 2 A g^{-1}	[12]
Layer by layer	0.1 M KCl – 3 electrodes	160 – 1 A g^{-1}	88 % - 2400 cycles – 3 A g^{-1}	This work
	0.1 M HCl – 3 electrodes	225 – 1 A g^{-1}		

To contextualize the specific capacitance results, Table S3 is presented. It includes specific capacitance values for PCZIF-8 electrodes reported in the literature, particularly those measured at a current density of 1 A g^{-1}. Although many reported studies utilize more corrosive electrolytes and extreme pHs, we standardized the current densities for our measurements to ensure a more equitable comparison. While our reported value is not among the highest, it is crucial to consider the advantages of the environmentally benign conditions under which these measurements were conducted.

Table S3- Supercapacitor performance comparison considering electrodes including PCZIF-8 with $C_{CG,SP}$ at 1 A g^{-1}.

Electrodes using PCZIF-8	Electrolyte	$C_{CG,SP}$ (F g^{-1}) / 1 A g^{-1}	Cycling Stability (GCD)	Reference
2 layers PCZIF-8-PANI	1 M H_2SO_4 3 electrodes	322	100 % - 10000 cycles – 5 mA s^{-1}	[13]
Core-shell PCZIF-8@PANI	1 M H_2SO_4 2 electrodes	236	86 % - 20000 cycles - 5 A g^{-1}	[14]
Co3O4 + PCZIF-8 and PANI polymerized outside	3 M KOH 3 electrodes	1407	87.7 % - 10000 cycles - 20 A g^{-1}	[15]
ZIF-8 + phytic acid is carbonized	6 M KOH 3 electrodes	219.4	100% - 2000 cycles – 5 A g^{-1}	[16]
CNC@ZIF-8 is carbonized	6 M KOH 3 electrodes	134	94.5% - 5000 cycles – 0.1 A g^{-1}	[17]
Layer by layer PCZIF-8/PANI:PSS	0.1 M KCl 3 electrodes	160	88 % - 2400 cycles – 3 A g^{-1}– 0.1M KCl	This work
	0.1 M HCl 3 electrodes	225		

References

1 J. Rouquerol, P. Llewellyn and F. Rouquerol, 2007, pp. 49–56.

2 D. A. Gómez-Gualdrón, P. Z. Moghadam, J. T. Hupp, O. K. Farha and R. Q. Snurr, *J. Am. Chem. Soc.*, 2016, **138**, 215–224.

3 S. Brunauer, P. H. Emmett and E. Teller, *J. Am. Chem. Soc.*, 1938, **60**, 309–319.

4 K. S. Park, Z. Ni, A. P. Cote, J. Y. Choi, R. Huang, F. J. Uribe-Romo, H. K. Chae, M. O'Keeffe and O. M. Yaghi, *Proc. Natl. Acad. Sci.*, 2006, **103**, 10186–10191.

5 L. Ren, G. Zhang, J. Lei, Y. Wang and D. Hu, *J. Colloid Interface Sci.*, 2018, **512**, 300–307.

6 J. Luo, Q. Ma, H. Gu, Y. Zheng and X. Liu, *Electrochim. Acta*, 2015, **173**, 184–192.

7 D.-W. Wang, F. Li, J. Zhao, W. Ren, Z.-G. Chen, J. Tan, Z.-S. Wu, I. Gentle, G. Q. Lu and H.-M. Cheng, *ACS Nano*, 2009, **3**, 1745–1752.

8 M. Hassan, K. R. Reddy, E. Haque, S. N. Faisal, S. Ghasemi, A. I. Minett and V. G. Gomes, *Compos. Sci. Technol.*, 2014, **98**, 1–8.

9 S. K. Simotwo, C. DelRe and V. Kalra, *ACS Appl. Mater. Interfaces*, 2016, **8**, 21261–21269.

10 T. P. Anandhu, R. R. Mohan, J. Cherusseri, R. R. and S. J. Varma, *Electrochim. Acta*, 2022, **425**, 140740.

11 S. K. Simotwo and V. Kalra, *Electrochim. Acta*, 2018, **268**, 131–138.

12 L.-J. Bian, F. Luan, S.-S. Liu and X.-X. Liu, *Electrochim. Acta*, 2012, **64**, 17–22.

13 A. Alameen, T. Jin, C. Xue, X. Ma, X. Du and X. Hao, *J. Solid State Electrochem.*, 2021, **25**, 777–787.

14 R. R. Salunkhe, J. Tang, N. Kobayashi, J. Kim, Y. Ide, S. Tominaka, J. H. Kim and Y. Yamauchi, *Chem. Sci.*, 2016, **7**, 5704–5713.

15 K. Chhetri, A. P. Tiwari, B. Dahal, G. P. Ojha, T. Mukhiya, M. Lee, T. Kim, S.-H. Chae, A. Muthurasu and H. Y. Kim, *J. Electroanal. Chem.*, 2020, **856**, 113670.

16 C. Guo, G. Li, Y. Wu, X. Wang, Y. Niu and J. Wu, *Energies*, 2023, **16**, 7232.

17 Y. Wang, T. Liu, X. Lin, H. Chen, S. Chen, Z. Jiang, Y. Chen, J. Liu, J. Huang and M. Liu, *ACS Sustain. Chem. Eng.*, 2018, **6**, 13932–13939.